

Intrinsic conformal order revealed in geometrically confined long-range repulsive particles

Zhenwei Yao*

*School of Physics and Astronomy, and Institute of Natural Sciences,
Shanghai Jiao Tong University, Shanghai 200240, China*

Elucidating long-range interaction guided organization of matter is a fundamental question in physical systems covering multiple length scales. Here, based on the hexagonal disk model, we analyze the characteristic inhomogeneity created by long-range repulsions, and reveal the intrinsic conformal order in particle packings in mechanical equilibrium. Specifically, we highlight the delicate angle-preserved bending of the lattice to match the inhomogeneity condition. The revealed conformal order is found to be protected by the surrounding topological defects. These results advance our understanding on long-range interacting systems, and open the promising possibilities of using long-range forces to create particle packings not accessible by short-range forces, which may have practical consequences.

I. INTRODUCTION

Long-range forces provide a unique mechanism to organize elementary constituents into a host of structures of multiple length scales that are not accessible by short-range forces [1, 2], ranging from self-gravitating systems [3, 4], plasmas [5, 6], elastic [7, 8] and hydrodynamic systems [9, 10], to the exceedingly rich electrostatic phenomena in electrolyte solutions [11–14]. Despite their ubiquity, the long-range coupling among the constituents imposes grand challenge for gaining insights into the resulting intriguing physics [15–17]. Studies on the packings of geometrically confined particles reveal the strong connection between long-range repulsion and inhomogeneity [18–22]. Analyzing the inhomogeneity phenomenon thus offers a promising perspective to study the fundamental physics of long-range interactions. This approach has proven fruitful, yielding the important concepts of curvature [19, 20, 23], topological defects [24–27], and conformal crystal [28–31] to uncover the featured geometric structures.

Previous studies show that long-range interactions create inhomogeneity in 2D packings of geometrically confined particles, where Gaussian curvature is induced and topological defects are excited to frustrate the crystalline order [19, 20, 25, 26]. However, the widely used rotationally symmetric confining potentials in both colloidal experiments and numerical simulations are incommensurate with the triangular lattice [19, 20, 32, 33]. This geometric incompatibility also leads to the frustration of the crystalline order, and thus obscures the intrinsic role of the physical interactions [5, 20, 24, 26, 34]. It is therefore natural to inquire into the assembly of particles purely dominated by the long-range interaction without any complication from the boundary. Revealing the intrinsic order in the inhomogeneous particle packings yields insights into the long-range interaction guided or-

ganization principle.

To address this question, we adopt the hexagonal geometry that is compatible with the triangular lattice, and focus on the mechanical evolution of the packing of the particles on a hexagonal disk under the long-range repulsive force at zero temperature. Furthermore, we let the total number of particles be a centered hexagonal number such that these particles may form a defect-free triangular lattice within a hexagonal disk. As such, the hexagonal disk model contains the essential elements for elucidating the intrinsic role of the long-range interaction in organizing particles [19].

Based on the hexagonal disk model, we perform numerical experiment to fully relax the particle configuration, and reveal the intrinsic conformal order in the resulting inhomogeneous equilibrium packings of particles under both regular and random initial conditions. Specifically, in the central defect-free zone (DFZ) we observe the delicate angle-preserved bending of the lattice (without breaking) to match the inhomogeneity condition. Surrounding the central DFZ, we discover the excitation of topological defects to resolve the intrinsic geometric frustration. The revealed conformal structure as protected by the surrounding defects represents a characteristic intrinsic order purely created by the long-range repulsion. These results advance our understanding on the fundamental physics of long-range interacting systems, and may have practical consequences in using long-range forces to control particle packings.

II. MODEL AND METHOD

The model system consists of a collection of interacting particles confined on a hexagonal disk. The interaction potential between particles is:

$$V(r) = \frac{\beta}{r^\Gamma}, \quad (1)$$

where Γ is an integer. The case of $\Gamma = 1$ corresponds to the long-range Coulomb potential in 3D space. We also

*Electronic address: zyao@sjtu.edu.cn

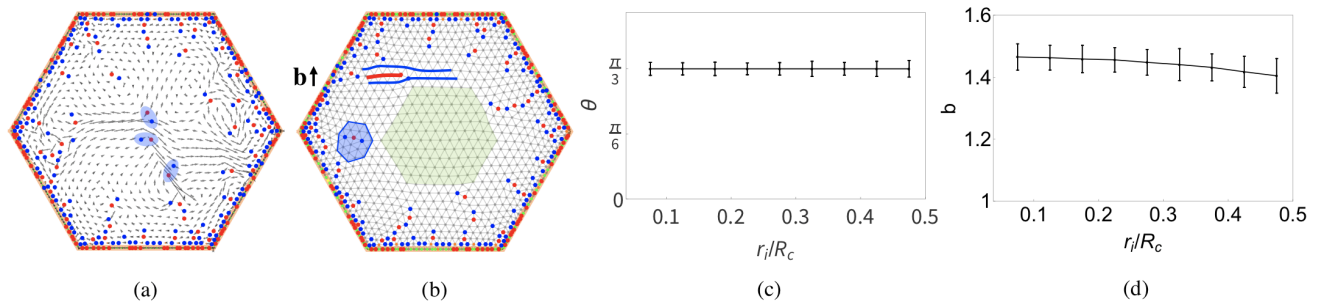


FIG. 1: Emergence of the conformal defect-free zone (DFZ) in the inhomogeneous equilibrium packing of the particles confined on the hexagonal disk. (a) and (b) Full relaxation of the system from the intermediate state (a) to the equilibrium state (b). A characteristic event is the energetically favored vanishing of the three dislocations as highlighted by the ovals in (a). The DFZ is indicated by the light green hexagon in (b). The colored dots represent different kinds of disclinations; the red and blue dots in the interior of the disk refer to five- and seven-fold disclinations. Panels (c) and (d) show the constancy of the bond angle θ as a signature of conformal transformation, and the shrinking of the bond length b towards the boundary. R_c is the radius of the inscribed circle of the hexagonal boundary. $N = 1141$.

investigate the cases of $\Gamma > 1$ for shorter-range interactions, and compare the results with the $1/r$ -Coulomb interaction. We shall point out that 2D Coulomb potential, as the Green's function for the 2D Poisson equation, scales logarithmically with distance. Here, we focus on the interaction potentials in the form of Eq.(1). One may also resort to the screened Coulomb potential (also known as the Yukawa potential) to investigate the effect of interaction range on the packing of particles; the effective screened Coulomb potential originates from the ions in electrolyte solution [35]. Note that universal structural behavior that is independent of the screening length has been reported in 2D Yukawa fluid based on the analysis of the pair correlation function [36].

Any particle that is outside the disk is subject to the confining potential:

$$V_{\text{conf.}}(r) = \frac{1}{2}k_0d^2, \quad (2)$$

where d is the shortest distance from the particle to the boundary, and k_0 reflects the stiffness of the potential. In simulations, the value of k_0 is set to be large enough [in comparison with β in Eq. (1)] to ensure that the particles are well confined within the disk. Due to the independence of the lowest-energy configuration on the value of β , we set $\beta = 1$ in simulations.

We employ the standard steepest descent method to determine the lowest-energy configurations in mechanical equilibrium without considering the thermal effect. The relaxation process consists of collective and individual movements of the particles under the force on each particle. The typical step size for these two kinds of relaxation modes are $s_c = 10^{-4}a_0$ and $s_i = 0.1s_c$, respectively. a_0 is the mean lattice spacing. Both regular and random initial conditions are considered. In the regular initial state, the particles in triangular lattice are arranged in concentric hexagons compatible with the hexagonal boundary. The total number of particles is $N = 3n(n-1)+1$, which is the n -th centered hexagonal number. Detailed infor-

mation about the numerical simulation is provided in the Supplemental Material.

III. RESULTS AND DISCUSSION

A. Identification of the central defect-free zone

We first discuss the case of Coulomb potential with $\Gamma = 1$ under the regular initial condition. It is found that the initially perfect triangular lattice is disrupted under the long-range repulsion as characterized by the excitation of the topological defects [see Fig. 1(a)]. The red and blue dots represent the fundamental five- and seven-fold disclinations; the defects are identified by the standard Delaunay triangulation procedure [25]. In a triangular lattice, a p -fold disclination refers to a point in the interior of the crystal with p neighbors, and it carries a topological charge of $q = 6 - z$ [25]. A pair of five- and seven-fold disclinations constitute a dislocation. The configuration in Fig. 1(a) is an intermediate state in the relaxation process. By further relaxing the configuration via individually updating particle positions, the system evolves towards the equilibrium state in Fig. 1(b). The displacement field is obtained from the deviation of the configurations in Fig. 1(a) and 1(b). The displacement of the particles is represented by the arrows in Figs. 1(a), which constitute a “flow” field. Comparison of Figs. 1(a) and 1(b) clearly shows that the central defects [indicated by the ovals in Fig. 1(a)] are swept away in the “flow”.

A salient feature of the equilibrium configuration in Fig. 1(b) is the emergence of the defect-free zone (DFZ, as highlighted by the light green hexagon) and the concentration of the geometric frustration near the boundary in the form of topological defects, including dislocations and the 7-5-7 defect strings that carry negative topological charge [as highlighted in the blue hexagon] [25]. The defects are located where the lattice is broken. For example, in Fig. 1(b) the distance between the two lattice

lines (in blue) is enlarged by one lattice spacing as they meet a dislocation (a pair of red and blue dots). The presence of the dislocation is to introduce an extra line of particles (on the red line) between the two lattice lines in blue. Consequently, the contour integral of the displacement field surrounding the dislocation in the lattice returns the Burgers vector \vec{b} . The direction of \vec{b} is indicated by the black arrow in Fig. 1(b).

For the crystallized particle array confined on a circular disk, the geometric incompatibility of the circular boundary and the interior triangular lattice could lead to the emergence of defects [19, 20, 26]. Here, in the hexagonal system without any boundary caused geometric incompatibility, the persistent boundary defects purely originate from the intrinsic density inhomogeneity created by the long-range repulsion. In other words, the increasing compression of the lattice towards the boundary, which is visible in the triangulated particle configuration in Fig. 1(b), leads to the disruption of the boundary crystalline zone and the proliferation of the defects. The long-range nature of the particle-particle interaction is crucial for this process.

According to the connection between topological defects and stress, the excitation of the boundary defects releases the stress in the system [37]. Consequently, the crystalline order in the central region is well preserved. In this sense, the central DFZ is protected by the surrounding defects. Here, it is of interest to mention that in polydispersed systems topological defects are excited surrounding an impurity particle of larger size to protect the crystalline order in the exterior region [38].

Numerical experiments show that the emergence of the DFZ requires a full relaxation of the system towards the energy valley with sufficiently fine step size. The energy is reduced by as small as 0.00174% as the system evolves from Fig. 1(a) to 1(b). The slight energy reduction is consistent with the fact that the relaxation process is dominated by the glide of dislocations, which requires a small amount of energy [25]. Note that the packing of charged point particles on a hexagonal disk has been investigated in our previous work, focusing on the total amount of interior topological charge Q_{int} [19]. Here, we adopt the relaxation procedure based on the combination of collective and individual movements of the particles under a finer simulation step, and reveal the DFZ structure in the lowest-energy particle configurations deeper in the energy valley. The total amount of interior topological charge Q_{int} is insensitive to the presence of the DFZ in the center of the hexagonal disk system.

To check the reliability of the numerical result in Fig. 1, we further reduce the value for s_i (the step size) down to $10^{-6}a_0$, and obtain the identical defect pattern as in Fig. 1(b). We also adjust the boundary stiffness by tuning the value of k_0 in Eq.(1), and find the persistence of the DFZ structure at varying values of k_0 . The relevant lowest-energy particle configurations are presented in the Supplemental Material.

B. Conformality of the central defect-free zone

To understand the formation of the DFZ in the environment of density inhomogeneity, we first analyze the radial distributions of the bond angle and the bond length. The results are presented in Figs. 1(c) and 1(d). It is found that from the center to the edge of the DFZ the mean bond length is appreciably decreased by about 5%. In contrast, the mean bond angle is a constant of $\pi/3$. As a signature of conformal transformation, the preservation of the bond angle suggests that the triangular lattice in the DFZ experiences a conformal deformation under the long-range repulsive force. Since the distribution of the bond angle is subject to a small fluctuation around $\pi/3$, the DFZ is essentially a conformal crystal in the statistical sense.

The notion of conformal crystal possesses an elegant mathematical structure under the continuous medium approximation [28–31]. In general, the conformal transformation is represented by an analytic function $\omega = f(z)$, where $z = x + iy$. $\omega = u(x, y) + iv(x, y)$. Any point (x_k, y_k) in the original triangular lattice on the (x, y) -plane is mapped to the point (u_k, v_k) on the (u, v) -plane. The distance ds_z of two points on the (x, y) -plane becomes ds_ω on the (u, v) -plane. By some calculation, we have

$$ds_\omega^2 = |\Lambda|^2 ds_z^2, \quad (3)$$

where $|\Lambda| = |d\omega/dz|$. By writing $ds_\omega^2 = ds_z^2 + 2\epsilon_{\alpha\beta} dx_\alpha dx_\beta$ where $x_1 = x$ and $x_2 = y$, and making use of the analyticity of $f(z)$, we obtain

$$\begin{aligned} \epsilon_{xx} &= \epsilon_{yy}, \\ \epsilon_{xy} &= \epsilon_{yx} = 0. \end{aligned} \quad (4)$$

The derivations of Eqs.(3) and (4) are presented in the Supplemental Material.

Equation (4) indicates that the conformal crystal could be obtained by a locally isotropic deformation (i.e., locally pure compression or stretching without any shear) of a perfect triangular lattice. The information of the density n_ω of the conformal crystal is encoded in the $|\Lambda|$ -factor. From the Jacobian of the transformation, we have

$$n_\omega = |\Lambda|^{-2} n_z, \quad (5)$$

where n_z is the density of the original triangular lattice. The analyticity of the conformal transformation dictates that the logarithm of the density of the conformal crystal conforms to the Laplace equation [31]:

$$\Delta \ln n_\omega = 0. \quad (6)$$

Equations (4) and (6) imply that the formation of conformal crystals requires subtle conditions. The deformation of the lattice shall simultaneously satisfy the density-inhomogeneity and the defect-free conditions. The concept of conformal crystal has been introduced in a neat experiment, where a collection of long-range

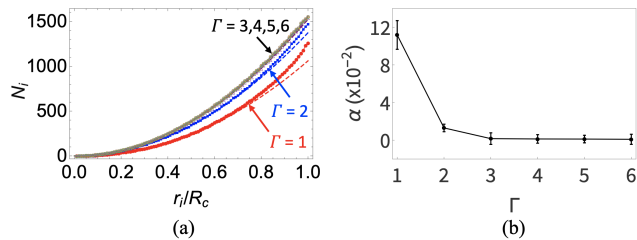


FIG. 2: Conformality of the central defect-free zone as characterized by the power-law density distribution. (a) Cumulative particle distribution $N(r)$ in the equilibrium configurations for different values of Γ . $N(r) \propto r^{2+\alpha}$ in the DFZ. $\alpha = 0.1$ and 0.013 for $\Gamma = 1$ and 2 , respectively. (b) The exponent α is plotted against the Γ -parameter. The error bars are obtained from the statistical analysis of the data for systems of varying n ($n = 20, 25, 30, 35, 40$). $N = 1141$.

repulsive magnetized spheres are self-organized into a regular nonuniform distribution named gravity's rainbow [28, 30]. But strictly conformal crystals are difficult to be realized; they could not be stabilized under uniform external field [31].

The rotationally symmetric solution to Eq.(6) conforms to: $n_\omega(r) = Cr^\alpha$, where C and α are constants. As such, in addition to the preserved bond angle, the power-law distribution of the density in the deformed lattice is also a signature of conformal crystals. To further examine the conformality of the DFZ, we analyze the radial distribution of the confined particles, and present the main results in Fig. 2. N_i is the number of particles within the circle of radius r_i . The particle density $n_\omega(r)$ is related to the cumulative particle distribution $N(r)$ by $n_\omega(r) = N'(r)/(2\pi r)$.

For the case of $\Gamma = 1$, Fig. 2(a) shows that the cumulative distribution in the DFZ conforms to the power law: $N(r) \propto r^{2+\alpha}$, where $\alpha = 0.10$. Therefore, the logarithm of the particle density in the DFZ conforms to the harmonic equation. The conformality of the DFZ is thus also confirmed in terms of the density distribution. Note that, since $N(r) \propto r^2$ for a uniform distribution, the parameter α serves as an indicator of the degree of inhomogeneity. The power-law density profile can be realized by the conformal transformation defined as $\omega = c'z^{1-\alpha/2}$ [21]. The demonstration of the conformal mappings is presented in the Supplemental Material.

In Fig. 2(a), we also present the cases of $\Gamma > 1$. The corresponding lowest-energy particle configurations at varying Γ are presented in Fig. 3. For $\Gamma = 2$, similar to the case of $\Gamma = 1$, we observe the emergence of the DFZ that is surrounded by the topological defects [see Fig. 3(b)]. The corresponding cumulative distribution in the DFZ could be well fitted by the power law with $\alpha = 0.013$. In contrast, Fig. 2(a) shows that the data for the cases of $\Gamma > 2$ collapse on the same fitting curve of the quadratic function. It indicates a homogeneous distribution of the particles, which is confirmed in numerical experiment; the lowest-energy particle configurations that

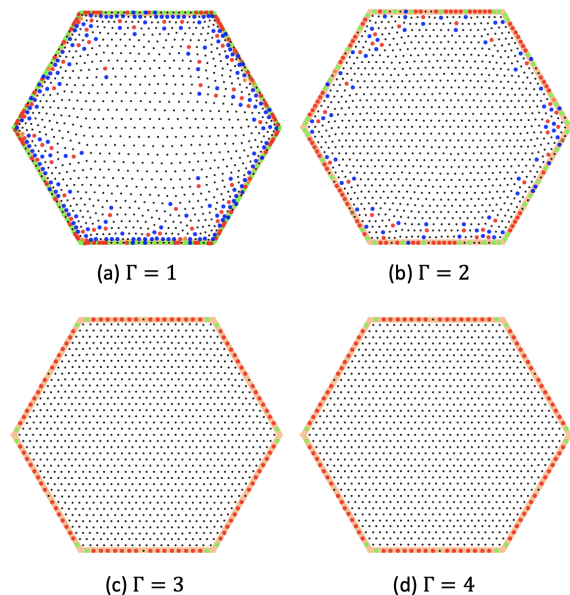


FIG. 3: Lowest-energy particle configurations at varying Γ . Topological defects emerge for the cases $\Gamma = 1$ and 2 . The red and blue dots in the interior of the disk represent five- and seven-fold disclinations. The equilibrium particle configurations for $\Gamma = 3$ or larger are free of defects. $N = 1141$.

are defect-free for $\Gamma = 3$ and 4 are presented in Fig. 3(c) and 3(d). As such, the cases of $\Gamma \leq 2$ are fundamentally different from the cases of larger Γ in terms of homogeneity. In the regime of long-range interaction ($\Gamma \leq 2$), the particle distribution becomes inhomogeneous, producing richer structures like the DFZ and the boundary defects.

To investigate the dependence of the degree of inhomogeneity as indicated by the value for α on the number of particles, we vary the value of N in the range from 1141 ($n = 20$) to 4681 ($n = 40$). The results are summarized in Fig. 2(b). The error bars are obtained from the statistical analysis of the data for systems of varying n . We see that the value for α is independent of the system size, and it is largely determined by the range of physical interaction.

Now, we analyze the characteristic distribution of density in the DFZ from the geometric perspective. Equation (3) shows that a line element in the original triangular lattice is isotropically expanded by a factor of $|\Lambda|$ by the conformal transformation. The $|\Lambda|$ -factor thus contains the information about the Gaussian curvature of the resulting conformal crystal according to the Gauss's Theorema Egregium. Given the metric in Eq. (3), one can derive for the Gaussian curvature [39]: $K_G = \frac{1}{|\Lambda|^2} \Delta \ln \left(\frac{1}{|\Lambda|} \right)$. In terms of the densities n_ω and n_z by Eq.(5), we have

$$K_G = \frac{n_\omega}{2n_z} \Delta \ln \left(\frac{n_\omega}{n_z} \right). \quad (7)$$

In combination with Eq.(6), we obtain an important property of the conformal crystal that its Gaussian cur-

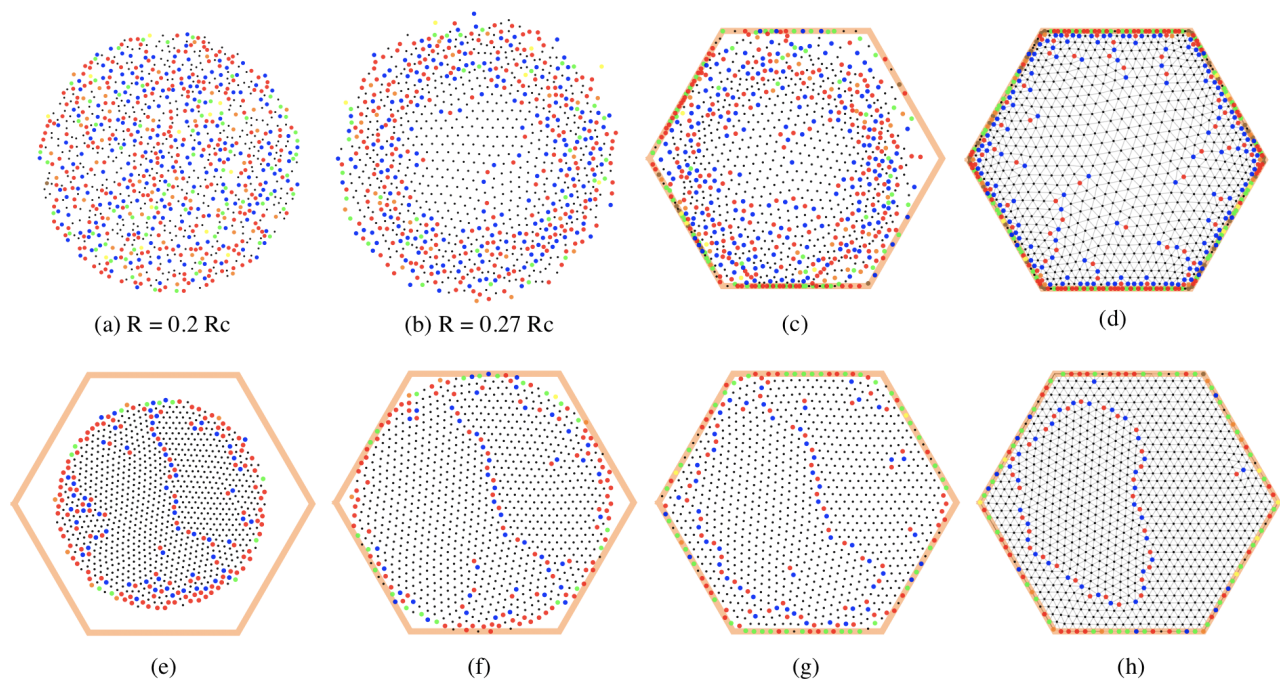


FIG. 4: Ordering process in both long- and short-range interacting systems under the random initial condition. Panels (a)-(d) and (e)-(h) show typical snapshots in the relaxation of the particle configurations for $\Gamma = 1$ and 6, respectively. For both kinds of cases, the particles are initially randomly distributed within a circle of radius R , and the rightmost panels show the equilibrium configurations. In (d), we observe the emergence of the central defect-free zone in the long-range repulsive system under the random initial condition. In (h), dislocations are spontaneously aggregated into a loop structure in the regime of short-range repulsion. $N = 1000$. R_c is the radius of the inscribed circle of the hexagonal boundary.

vature is zero. In general, non-uniform deformation of a perfect triangular lattice leads to the variation of the metric, and thus gives rise to a nonzero intrinsic Gaussian curvature. The conformal crystal sets the remarkable example of realizing zero curvature in the environment of inhomogeneity. Previous studies show that the overall geometric effect of the long-range repulsion is to induce nonzero Gaussian curvature in the inhomogeneous planar particle arrays [19, 20, 26, 40]. Here, in the hexagonal system we reveal the zero-curvature domain, where the bond-orientational order is well preserved, and the particle distribution conforms to the power law [25].

We further analyze the DFZ structure by resorting to the fundamental relation between particle density and topological charge density in two-dimensional crystals [25]. Geometric analysis shows that the topological charge density is proportional to $\Delta \ln n_\omega$ [26]. Therefore, Eq.(6) is also recognized as the condition of zero topological charge density. To conclude, the preceding discussions lead to a clear physical scenario about the organization of geometrically confined long-range repulsive particles. In the central region, the particles adopt the defect-free conformal organization, where the lattice subtly bends to match the inhomogeneity condition without breaking [23]. The disruption of the crystalline order mainly occurs near the boundary, where the excited topological defects serve as stress-releasers to protect the

conformal order in the central region.

Systematic simulations under a series of random initial conditions show that the coexistence of the conformal DFZ and the defective boundary region is a common phenomenon in the long-range interacting hexagonal systems. Specifically, we confine randomly distributed particles within circular regions of varying radius R . Let R_c be the radius of the inscribed circle of the hexagonal boundary. R/R_c ranges from 0.2 to 0.9. Typical particle configurations in the relaxation process are presented in the upper panels in Fig. 4. A key observation is that, in the free expansion of the circular cluster of particles, ordering is initiated from the central region [see Figs. 4(a) and 4(b)]. The central region ultimately becomes free of defects in the equilibrium state in Fig. 4(d). In all of the cases with varying R , we uniformly observe the appearance of the DFZ in the equilibrium configurations. In contrast, for short-range interacting systems, by changing the initial condition from the regular triangular lattice to random configurations, we observe the self-organization of dislocations into the loop structure. Typical configurations in the relaxation process for $\Gamma = 6$ are presented in the lower panels in Fig. 4. The resulting dislocation-fabricated loop separates the entire lattice into two crystallites as shown in Fig. 4(h). More information about the formation of the loop structure is provided in the Supplemental Material.

IV. CONCLUSION

In summary, we investigate the fundamental question about the assembly of particles under the long-range interaction, and reveal the intrinsic conformal order in the inhomogeneous equilibrium packings. Specifically, the geometrically confined particles are steered by the long-range repulsion to form a conformal defect-free zone as protected by surrounding topological defects. Around the inhomogeneous defect-free zone, we discuss the remarkable confluence of the deeply connected notions of conformality, harmonic inhomogeneity, zero curvature,

and zero topological charge density. This work demonstrates the long-range interaction guided organization of matter, and may inspire further explorations into the intriguing geometric structures underlying the long-range interaction driven inhomogeneity.

Acknowledgments

This work was supported by the National Natural Science Foundation of China (Grants No. BC4190050).

-
- [1] A. Campa, T. Dauxois, D. Fanelli, and S. Ruffo, *Physics of Long-Range Interacting Systems* (Oxford University Press, Oxford, UK, 2014).
 - [2] Y. Levin, R. Pakter, F. B. Rizzato, T. N. Teles, and F. P. Benetti, *Phys. Rep.* **535**, 1 (2014).
 - [3] T. Padmanabhan, *Phys. Rep.* **188**, 285 (1990).
 - [4] F. P. Benetti, A. C. Ribeiro-Teixeira, R. Pakter, and Y. Levin, *Phys. Rev. Lett.* **113**, 100602 (2014).
 - [5] H. Thomas, G. Morfill, V. Demmel, J. Goree, B. Feuerbacher, and D. Möhlmann, *Phys. Rev. Lett.* **73**, 652 (1994).
 - [6] Y. Levin, *Rep. Prog. Phys.* **65**, 1577 (2002).
 - [7] L. D. Landau and E. M. Lifshitz, *Theory of Elasticity, 3rd edition* (Butterworth-Heinemann, 1986).
 - [8] B. Audoly and Y. Pomeau, *Elasticity and geometry* (Oxford Univ. Press, 2010).
 - [9] S. Chattopadhyay and X.-L. Wu, *Biophys. J.* **96**, 2023 (2009).
 - [10] M. C. Dallaston, M. A. Fontelos, D. Tseluiko, and S. Kalliadasis, *Phys. Rev. Lett.* **120**, 034505 (2018).
 - [11] C. Holm, P. Kékicheff, and R. Podgornik, *Electrostatic Effects in Soft Matter and Biophysics* (Springer, Berlin, 2001).
 - [12] D. A. Walker, B. Kowalczyk, M. Olvera de la Cruz, and B. A. Grzybowski, *Nanoscale* **3**, 1316 (2011).
 - [13] V. Lee, S. R. Waitukaitis, M. Z. Miskin, and H. M. Jaeger, *Nat. Phys.* **11**, 733 (2015).
 - [14] H. Shen, H. Tong, P. Tan, and L. Xu, *Nat. Commun.* **10**, 1 (2019).
 - [15] V. A. Schweigert and F. M. Peeters, *Phys. Rev. B* **51**, 7700 (1995).
 - [16] E. Oğuz, R. Messina, and H. Löwen, *Europhys. Lett.* **94**, 28005 (2011).
 - [17] A. C. Ribeiro-Teixeira, F. P. Benetti, R. Pakter, and Y. Levin, *Phys. Rev. E* **89**, 022130 (2014).
 - [18] A. Berezin, *Nature* **315**, 104 (1985).
 - [19] Z. Yao and M. Olvera de la Cruz, *Phys. Rev. Lett.* **111**, 115503 (2013).
 - [20] V. Soni, L. R. Gómez, and W. T. Irvine, *Phys. Rev. X* **8**, 011039 (2018).
 - [21] F. C. Silva, R. M. Menezes, L. R. Cabral, and C. C. de Souza Silva, *J. Phys.: Condens. Matter* **32**, 505401 (2020).
 - [22] H. Sun and Z. Yao, *Phys. Rev. E* **108**, 025001 (2023).
 - [23] A. Mughal and D. Weaire, *Proc. R. Soc. London, Ser. A* **465**, 219 (2009).
 - [24] Y.-J. Lai and I. Lin, *Phys. Rev. E* **60**, 4743 (1999).
 - [25] D. R. Nelson, *Defects and Geometry in Condensed Matter Physics* (Cambridge University Press, Cambridge, 2002).
 - [26] A. Mughal and M. Moore, *Phys. Rev. E* **76**, 011606 (2007).
 - [27] B. A. Klumov, *JETP Letters* **116**, 703 (2022).
 - [28] P. Pierański, in *Phase Transitions in Soft Condensed Matter* (Springer, 1989), pp. 45–48.
 - [29] F. Rothen, P. Pieranski, N. Rivier, and A. Joyet, *Eur. J. Phys.* **14**, 227 (1993).
 - [30] F. Rothen and P. Pierański, *Phys. Rev. E* **53**, 2828 (1996).
 - [31] K. W. Wojciechowski and J. Klos, *J. Phys. A: Math. Gen.* **29**, 3963 (1996).
 - [32] B. A. Klumov, *JETP Letters* **110**, 715 (2019).
 - [33] Q. Meng and G. M. Grason, *Phys. Rev. E* **104**, 034614 (2021).
 - [34] C. B. S. Nesar, T. Palberg and P. Leiderer, *Prog. Colloid Polym. Sci.* **104**, 194 (1997).
 - [35] Z. Yao, *Europhys. Lett.* **133**, 54002 (2021).
 - [36] B. A. Klumov, *JETP Letters* **115**, 108 (2022).
 - [37] P. Chaikin and T. Lubensky, *Principles of Condensed Matter Physics* (Cambridge University Press, 1995).
 - [38] Z. Yao and M. Olvera de la Cruz, *Proc. Natl. Acad. Sci. U.S.A.* **111**, 5094 (2014).
 - [39] D. Struik, *Lectures on Classical Differential Geometry* (Dover Publications, New York, 1988), 2nd ed.
 - [40] D. Nelson and L. Peliti, *J. Phys. (France)* **48**, 1085 (1987).